Title
Hybrid simulation theory for a classical nonlinear dynamical system

Authors
Drazin, Paul L
Govindjee, Sanjay

Publication Date
2017-03-01

DOI
10.1016/j.jsv.2016.12.034

Peer reviewed

Journal of Sound and Vibration ∎ (∎∎∎∎) ∎∎∎–∎∎∎

Contents lists available at ScienceDirect

Journal of Sound and Vibration

journal homepage: www.elsevier.com/locate/jsvi

Hybrid simulation theory for a classical nonlinear dynamical system

Paul L. Drazin [a], Sanjay Govindjee [b,*]

[a] Department of Mechanical Engineering, University of California, Berkeley, Berkeley, CA 94720, United States
[b] Department of Civil and Environmental Engineering, University of California, Berkeley, Berkeley, CA 94720, United States

ARTICLE INFO

Article history:
Received 23 June 2016
Received in revised form
17 November 2016
Accepted 20 December 2016

Keywords:
Hybrid simulation
Hybrid simulation error analysis
Nonlinear dynamics
Chaos
Lyapunov exponent
Lyapunov dimension
Poincaré section

ABSTRACT

Hybrid simulation is an experimental and computational technique which allows one to study the time evolution of a system by physically testing a subset of it while the remainder is represented by a numerical model that is attached to the physical portion via sensors and actuators. The technique allows one to study large or complicated mechanical systems while only requiring a subset of the complete system to be present in the laboratory. This results in vast cost savings as well as the ability to study systems that simply can not be tested due to scale. However, the errors that arise from splitting the system in two requires careful attention, if a valid simulation is to be guaranteed. To date, efforts to understand the theoretical limitations of hybrid simulation have been restricted to linear dynamical systems. In this work we consider the behavior of hybrid simulation when applied to nonlinear dynamical systems. As a model problem, we focus on the damped, harmonically-driven nonlinear pendulum. This system offers complex nonlinear characteristics, in particular periodic and chaotic motions. We are able to show that the application of hybrid simulation to nonlinear systems requires a careful understanding of what one expects from such an experiment. In particular, when system response is chaotic we advocate the need for the use of multiple metrics to characterize the difference between two chaotic systems via Lyapunov exponents and Lyapunov dimensions, as well as correlation exponents. When system response is periodic we advocate the use of L^2 norms. Further, we are able to show that hybrid simulation can falsely predict chaotic or periodic response when the true system has the opposite characteristic. In certain cases, we are able to show that control system parameters can mitigate this issue.

1. Introduction

Hybrid simulation (or hybrid-testing) is a popular experimental method that is primarily used in Civil Engineering laboratories [1,2]. It originated roughly 30 years ago [3] and has been used continuously and extensively as a methodology to experimentally assess structural systems under earthquake loadings. Occasionally the methodology has also been used in other disciplines to assess dynamic phenomena; see e.g. [4–6]. The central problem that hybrid simulation addresses is that it is very difficult and expensive to test full-size civil structures for their structural capacities under seismic loads. The largest testing facility in the world is the E-Defense facility [7] which can test structures with a 20 m × 15 m plan and 12 MN

* Corresponding author.
E-mail addresses: pdrazin@berkeley.edu (P.L. Drazin), s_g@berkeley.edu (S. Govindjee).

http://dx.doi.org/10.1016/j.jsv.2016.12.034
0022-460X/

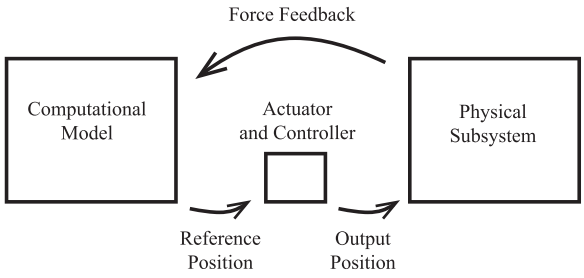

Fig. 1. A simple diagram of a hybrid system setup.

weight. While this represents a large capacity, it precludes the testing of many types of structures, is very expensive due to the need to build full-size prototypes, has limited throughput, and does not easily allow for design exploration.

At its heart, one can think of experimental testing of this variety as the use of an analog computer (algorithm) to simulate the behavior of a structure. Hybrid testing and its many variants (see e.g. [8,9]) tries to leverage this viewpoint in the following manner: (1) The determination of the dynamic response of a structural system is thought of as the integration of the equations of motion for the structure; (2) The integration of the system of equations is done by a hybrid mix of numerical and analog computing. In practice, this means that part of the structural system is physically present in the laboratory and the remainder is represented by a computer model. Both parts of the structure are subjected to dynamic excitation and they interact via a system of sensors and actuators in real- and/or pseudo-time [10]. Fig. 1 provides a schematic of the setup. Its advantage comes about when one can place the bulk of the structure in the computer due to a confidence in its model; the physical part typically represents a subset of the structure for which one does not have a good model; see e.g. [11].

Despite the long history of hybrid-testing, very little is understood about the theoretical errors involved when one uses this methodology to simulate the response of a structure. The bulk of the literature on hybrid-testing has focused on improving the accuracy and speed of the numerical computation and the fidelity of the control system [12–14] – all with the implicit assumption that improvements in these aspects will render a result that is more faithful to an untested physical reality. There have also been attempts to see how the location of the hybrid interface can affect the overall dynamics of the hybrid system [15]. Recently, however, efforts have been put forth to try and understand the theoretical limitations of hybrid testing [16,17] independent of the systematic and random errors that arise from numerical issues and sensor errors. These works utilized a reference structural system that was fully theoretical, split the system into fictitious physical and computational parts, and then explored the fidelity of the hybrid equations with respect to the reference equations. In this way, the true dynamical response of the reference system was known *a priori* in analytic form and could be compared to the hybrid-system response which was also known in analytic form. The overall methodology thus illuminated directly the central feature of all hybrid simulation methodologies – viz., the presence of a split system that is patched together with an imperfect interface.

The works of [16,17] focused on two linear structural systems – Euler-Bernoulli beams (elastic and viscoelastic) and Kirchhoff-Love plates (elastic). In this paper, we attempt to extend this analysis framework to a nonlinear dynamical system in order to understand the behavior of hybrid-simulation in the presence of kinematic nonlinearities. We solely consider the *theoretical* performance of real-time hybrid simulation as an experimental method, ignoring all of the numerical and random errors, as this leads to a best case scenario for a hybrid experiment; see e.g. [2] or [18]. This approach eliminates the errors associated with time integration methods and signal noise and focuses only on the errors that are generated by systematic interface mismatch errors – an element that is always present in hybrid simulations. As a model problem we focus upon the damped, driven nonlinear pendulum; see [19] for an in depth analysis of the dynamics of this system. This system is one of the most basic nonlinear systems that has a clear physical representation. Despite the simplicity of this system, it has a wide variety of properties that make it interesting to study. For instance, this system exhibits a rich dynamical response with both periodic and chaotic trajectories. We can use these two behaviors to help us study how a hybrid split affects the overall dynamics of a nonlinear mechanical system. We also include a spring-mass-damper actuator system which is controlled by a PI controller. This setup for the hybrid system gives a more advanced representation of the hybrid system in comparison to the constant error methodology used in [16,17].

2. General theory of hybrid simulation

In this section we will set up a general framework for thinking about hybrid simulation.

2.1. The reference system

First, we need to set up the reference system to which the hybrid system will be compared. A mechanical system with domain $\mathcal{D}$ is considered, as shown in Fig. 2a. The mechanical response of the system is characterized by a state vector,

Please cite this article as: P.L. Drazin, & S. Govindjee, Hybrid simulation theory for a classical nonlinear dynamical system, *Journal of Sound and Vibration* (2016), http://dx.doi.org/10.1016/j.jsv.2016.12.034

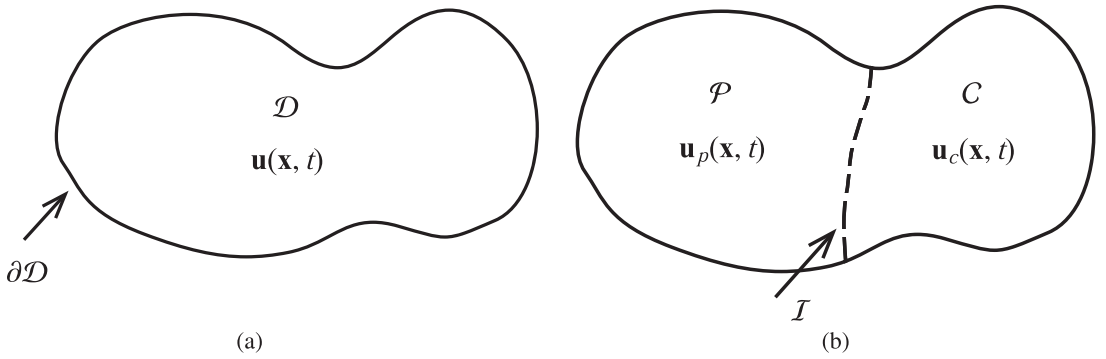

Fig. 2. (a) A general system with domain $\mathcal{D}$ and state vector $\mathbf{u}(\mathbf{x}, t)$. (b) A general system with imposed separation into two substructures for comparison to the hybrid system. $\mathcal{P} \cup \mathcal{I} \cup \mathcal{C} = \mathcal{D}$ and $\partial\mathcal{P} \cap \partial\mathcal{C} = \mathcal{I}$.

$$\mathbf{u}(\mathbf{x}, t) \text{ for } \mathbf{x} \in \mathcal{D}, \tag{1}$$

where t represents time. In order to compare the reference system response to the hybrid system response, we imagine that the reference system is split into two substructures: a "physical" substructure ($\mathcal{P}$-side) and a "computational" substructure ($\mathcal{C}$-side) as shown in Fig. 2b, where $\mathcal{P} \cup \mathcal{I} \cup \mathcal{C} = \mathcal{D}$ and $\partial\mathcal{P} \cap \partial\mathcal{C} = \mathcal{I}$. The state vector can now be separated into two parts:

$$\mathbf{u}(\mathbf{x}, t) = \begin{cases} \mathbf{u}_p(\mathbf{x}, t) & \text{if } \mathbf{x} \in \mathcal{P} \\ \mathbf{u}_c(\mathbf{x}, t) & \text{if } \mathbf{x} \in \mathcal{C}. \end{cases} \tag{2}$$

This defines the true response for a given mechanical system . The precise expression for $\mathbf{u}(\mathbf{x}, t)$ is found by determining the function that satisfies the governing equations of motion on $\mathcal{D}$ and the imposed boundary conditions on $\partial\mathcal{D}$.

2.2. The hybrid system

The response of the hybrid system should be defined in a similar fashion to make the comparison between the two systems straight forward. Using the same boundary defined in Fig. 2b, the hybrid system is separated into two substructures, as seen in Fig. 3. In order to differentiate the reference system from the hybrid system a superposed hat ($\hat{}$) is used to indicate a quantity in the hybrid system. The mechanical response of the hybrid system is represented by the following state vector:

$$\hat{\mathbf{u}}(\mathbf{x}, t) = \begin{cases} \hat{\mathbf{u}}_p(\mathbf{x}, t) & \text{if } \mathbf{x} \in \mathcal{P} \\ \hat{\mathbf{u}}_c(\mathbf{x}, t) & \text{if } \mathbf{x} \in \mathcal{C}. \end{cases} \tag{3}$$

In a hybrid system $\hat{\mathbf{u}}_p$ and $\hat{\mathbf{u}}_c$ are determined from the "solution" of the governing equations of motion for $\mathcal{P}$ and $\mathcal{C}$ subjected to the boundary conditions on $\partial\mathcal{P}$ and $\partial\mathcal{C}$. The boundary conditions on $\partial\mathcal{D} \cap \partial\mathcal{P}$ and $\partial\mathcal{D} \cap \partial\mathcal{C}$ naturally match those of the reference system. However, in the hybrid system one must additionally deal with boundary conditions on the two interface sides $\mathcal{I}_p$ and $\mathcal{I}_c$, where $\mathcal{I}_p = \mathcal{I} \cap \partial\mathcal{P}$ and $\mathcal{I}_c = \mathcal{I} \cap \partial\mathcal{C}$. The boundary conditions on $\mathcal{I}_p$ and $\mathcal{I}_c$ are provided by the sensor and actuator system.

The hybrid split leads to more unknowns than equations. To resolve this issue, we need a model of the actuator and sensor system. A relatively general form for such a model can be expressed as [16]:

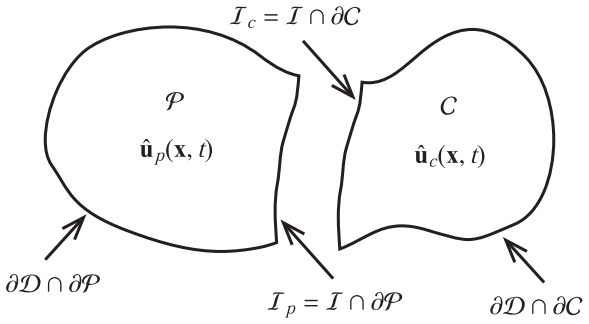

Fig. 3. The hybrid system separated into the physical, $\mathcal{P}$, and computational, $\mathcal{C}$, substructures.

Please cite this article as: P.L. Drazin, & S. Govindjee, Hybrid simulation theory for a classical nonlinear dynamical system, *Journal of Sound and Vibration* (2016), http://dx.doi.org/10.1016/j.jsv.2016.12.034

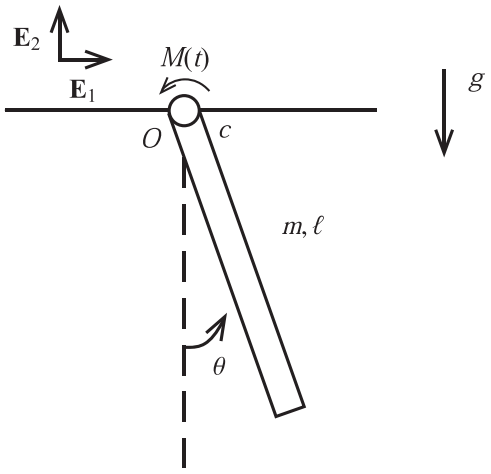

Fig. 4. The damped, driven nonlinear pendulum with a rigid body rotating about O with applied moment $M(t)$.

$$\underline{D}_c[\hat{\mathbf{u}}_c]\Big|_{I_c} = \underline{D}_p[\hat{\mathbf{u}}_p]\Big|_{I_p}, \tag{4}$$

where $\underline{D}_c[\bullet]$ and $\underline{D}_p[\bullet]$ are operators that generate the necessary equations at the interface from the state vectors $\hat{\mathbf{u}}_\bullet$. Later in this paper, a simple spring-mass damper system with a PI controller will be used to model the interface, and thus allows us to precisely specify the form of $\underline{D}_c[\bullet]$ and $\underline{D}_p[\bullet]$. This model allows one to study the effects of systematic hybrid system splitting errors, specifically boundary mismatch errors. Such errors directly correlate to errors seen in experimental hybrid systems; see e.g. [2] or [20].

In an actual hybrid simulation, one only has the physical part $\mathcal{P}$, the sensor and actuator system, and the computational model for part $\mathcal{C}$. This makes it challenging to know if the determined response $\hat{\mathbf{u}}$ is correct to a sufficient degree. To circumvent this issue we will work with an analytical model for part $\mathcal{P}$ and part $\mathcal{C}$ as well as for the sensor and actuator system. This will allow us to faithfully compute the error in the response quantity $\hat{\mathbf{u}}$ of the hybrid system by comparing it to the response quantity $\mathbf{u}$ of the reference system. The error investigated is then strictly the error in the hybrid system associated with the splitting interface.

3. Damped, driven nonlinear pendulum

3.1. The reference system

The first system that is discussed in this paper is that of the reference damped, driven nonlinear pendulum; a diagram of which is shown in Fig. 4.

The pendulum consists of a uniform rigid rod of mass m and length ℓ that rotates about the point O. There is an applied moment $M(t)$ at O, and there is linear viscous damping at O with damping constant c. The kinetic energy of the system is given by

$$T = \frac{m\ell^2}{6}\dot{\theta}^2, \tag{5}$$

and the potential energy is given by

$$U = mg\left(\frac{\ell}{2} - \frac{\ell}{2}\cos(\theta)\right). \tag{6}$$

Using Lagrange's prescription for finding the equations of motion (see e.g. [21]) one has

$$\frac{d}{dt}\left(\frac{\partial T}{\partial \dot{\theta}}\right) - \frac{\partial T}{\partial \theta} + \frac{\partial U}{\partial \theta} = M_{nc}, \tag{7}$$

where

$$M_{nc} = -c\dot{\theta} + M(t). \tag{8}$$

This gives

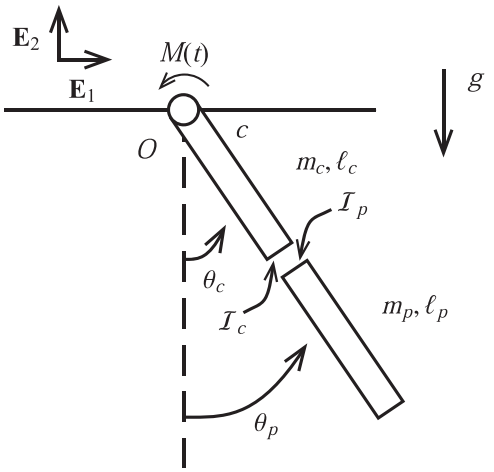

Fig. 5. The hybrid pendulum with the rigid body split into two pieces rotating about O with applied moment $M(t)$.

$$\frac{m\ell^2}{3}\ddot{\theta} + c\dot{\theta} + mg\frac{\ell}{2}\sin(\theta) = M(t), \tag{9}$$

the equation that determines the true motion of the system.

3.2. The hybrid system

Next, we set-up the hybrid pendulum; a diagram of which is shown in Fig. 5. In this case, the rigid body is split into two distinct bodies that have distinct angles of rotation θ_c and θ_p, but both bodies still rotate about O. Also, we have that the lengths $\ell_p + \ell_c = \ell$, and the masses $m_p = \frac{\ell_p}{\ell}m$, $m_c = \frac{\ell_c}{\ell}m$, and thus $m_p + m_c = m$. The kinetic energy is given by

$$\hat{T} = \frac{m_c\ell_c^2}{6}\dot{\theta}_c^2 + \left(\frac{m_p\ell_p^2}{6} + \frac{m_c\ell_p^2 + m_p\ell_c^2}{2}\right)\dot{\theta}_p^2, \tag{10}$$

and the potential energy is given by

$$\hat{U} = m_c g\left(\frac{\ell_c}{2} - \frac{\ell_c}{2}\cos(\theta_c)\right) + m_p g\left(\left(\ell_c + \frac{\ell_p}{2}\right) - \left(\ell_c + \frac{\ell_p}{2}\right)\cos(\theta_p)\right), \tag{11}$$

where the hat, $\hat{\bullet}$, represents a quantity in the hybrid system. We apply Lagrange's prescription with respect to θ_c and θ_p, which is

$$\frac{d}{dt}\left(\frac{\partial\hat{T}}{\partial\dot{\theta}_i}\right) - \frac{\partial\hat{T}}{\partial\theta_i} + \frac{\partial\hat{U}}{\partial\theta_i} = \hat{M}_{nci}, \tag{12}$$

for $i = c, p$, where

$$\hat{M}_{ncc} = -c\dot{\theta}_c + M(t) + M_c, \quad \hat{M}_{ncp} = M_p. \tag{13}$$

Here, M_c is the moment at $\mathcal{I}_c$ and M_p is the moment at $\mathcal{I}_p$. In this setup, M_c is an input to the computational model and M_p is measured by sensors. Expanding Eq. (12) we get

$$\frac{m_c\ell_c^2}{3}\ddot{\theta}_c + c\dot{\theta}_c + m_c g\frac{\ell_c}{2}\sin(\theta_c) = M(t) + M_c, \tag{14}$$

and

$$\left(\frac{m_p\ell_p^2}{3} + m_c\ell_p^2 + m_p\ell_c^2\right)\ddot{\theta}_p + m_p g\left(\ell_c + \frac{\ell_p}{2}\right)\sin(\theta_p) = M_p. \tag{15}$$

We note that, in the ideal setting with no sensor error, $M_c = -M_p$. We make this assumption so we can focus on the systematic errors rather than sensor errors. Doing so allows us to combine Eqs. (14) and (15) into a single equation, given by

Please cite this article as: P.L. Drazin, & S. Govindjee, Hybrid simulation theory for a classical nonlinear dynamical system, *Journal of Sound and Vibration* (2016), http://dx.doi.org/10.1016/j.jsv.2016.12.034

$$\frac{m_c\ell_c^2}{3}\ddot{\theta}_c + \left(\frac{m_p\ell_p^2}{3} + m_c\ell_p^2 + m_p\ell_c^2\right)\ddot{\theta}_p + c\dot{\theta}_c + m_c g\frac{\ell_c}{2}\sin(\theta_c) + m_p g\left(\ell_c + \frac{\ell_p}{2}\right)\sin(\theta_p) = M(t). \tag{16}$$

However, at this point, we only have one equation, Eq. (16), and two unknowns, θ_c and θ_p. To get a second equation, we need a model for the sensor and actuator system that connects the two bodies. For this paper, this is modeled as a spring-mass-damper system controlled by a PI controller; see e.g. [22]. The use a spring-mass-damper was chosen purely for its mechanical simplicity and ease of understanding. The spring-mass-damper system can be easily used to introduce phase and magnitude errors – known hybrid simulation errors [2,14,13] – at the hybrid interface while still allowing one to have an analytical model that can be solved using standard numerical techniques, such as the Runge-Kutta methods. For the model chosen, we follow the definition from the previous section for internal boundary conditions, or

$$\underline{D}_c[\hat{\mathbf{u}}_c]\Big|_{I_c} = \underline{D}_p[\hat{\mathbf{u}}_p]\Big|_{I_p}. \tag{17}$$

In this case $\hat{\mathbf{u}}_c$ and $\hat{\mathbf{u}}_p$ are given by

$$\hat{\mathbf{u}}_c = \left[\theta_c\right], \quad \hat{\mathbf{u}}_p = \left[\theta_p\right], \tag{18}$$

and the operators $\underline{D}_c[\hat{\mathbf{u}}_c]$ and $\underline{D}_p[\hat{\mathbf{u}}_p]$ have the following definitions:

$$\underline{D}_c[\hat{\mathbf{u}}_c] = \left(k_a k_i + \left(k_a k_p + c_a k_i\right)\frac{d}{dt} + c_a k_p\frac{d^2}{dt^2}\right)\hat{\mathbf{u}}_c, \tag{19}$$

and

$$\underline{D}_p[\hat{\mathbf{u}}_p] = \left(k_a k_i + \left(k_a(1+k_p) + c_a k_i\right)\frac{d}{dt} + \left(c_a(1+k_p)\right)\frac{d^2}{dt^2} + m_a\frac{d^3}{dt^3}\right)\hat{\mathbf{u}}_p, \tag{20}$$

where the parameters m_a, c_a, and k_a are the mass, damping constant, and stiffness of the spring-mass-damper system used to model the actuator. The parameters k_p and k_i are the proportional and integral gains of the PI controller. Applying these definitions ultimately leads to

$$c_a k_p\ddot{\theta}_c + (k_a k_p + c_a k_i)\dot{\theta}_c + k_a k_i\theta_c = m_a\ddot{\theta}_p + (c_a(1+k_p))\ddot{\theta}_p + (k_a(1+k_p) + c_a k_i)\dot{\theta}_p + k_a k_i\theta_p. \tag{21}$$

Thus, the equations of motion for the hybrid system are given by Eqs. (16) and (21). While the PI controller has been used in previous works [5], it is emphasized that the PI controller is only used here for concreteness. The entire exercise is easily repeatable with alternate control methodologies; see e.g. [23,11]. The controller that one should employ in an actual experiment is based on the experimental setup that is used and one that minimizes errors that are important to problem at hand (amongst those metrics that we highlight in the paper and perhaps others of physical significance to the researcher). For these reasons, alternative control schemes are not discussed further in this paper.

3.3. Non-dimensionalization

For further analysis, it is beneficial to non-dimensionalize Eqs. (9), (16), and (21). In order to do this, we define the following non-dimensional quantities:

$$\tau = t\sqrt{\frac{g}{\ell}}, \tag{22a}$$

$$L_c = \frac{\ell_c}{\ell}, \quad L_p = \frac{\ell_p}{\ell}, \tag{22b}$$

$$M_c = \frac{m_c}{m} = L_c, \quad M_p = \frac{m_p}{m} = L_p, \tag{22c}$$

$$\gamma = \frac{c}{m\ell\sqrt{g\ell}}, \tag{22d}$$

$$\mu(\tau) = \frac{M\left(t = \tau\sqrt{\frac{\ell}{g}}\right)}{mg\ell}, \tag{22e}$$

$$M_a = \frac{m_a}{m}, \quad \gamma_a = \frac{c_a}{m}\sqrt{\frac{\ell}{g}}, \quad K_a = \frac{k_a \ell}{mg}, \tag{22f}$$

$$K_p = k_p, \quad K_i = k_i\sqrt{\frac{\ell}{g}}. \tag{22g}$$

Using Eq. (22) allows us to rewrite Eqs. (9), (16), and (21) as,

$$\frac{d^2\theta}{d\tau^2} + 3\gamma\frac{d\theta}{d\tau} + \frac{3}{2}\sin(\theta) = 3\mu(\tau), \tag{23}$$

$$\frac{L_c^3}{3}\frac{d^2\theta_c}{d\tau^2} + \left(\frac{L_p^3}{3} + L_c L_p\right)\frac{d^2\theta_p}{d\tau^2} + \gamma\frac{d\theta_c}{d\tau} + \frac{L_c^2}{2}\sin(\theta_c) + \left(L_p L_c + \frac{L_p^2}{2}\right)\sin(\theta_p) = \mu(\tau), \tag{24}$$

and

$$\gamma_a K_p\frac{d^2\theta_c}{d\tau^2} + (K_a K_p + \gamma_a K_i)\frac{d\theta_c}{d\tau} + K_a K_i\theta_c = M_a\frac{d^3\theta_p}{d\tau^3} + (\gamma_a(1+K_p))\frac{d^2\theta_p}{d\tau^2} + (K_a(1+K_p) + \gamma_a K_i)\frac{d\theta_p}{d\tau} + K_a K_i\theta_p. \tag{25}$$

This gives us the non-dimensionalized equations of motion for the reference and hybrid systems.

4. Analysis

For the analysis, the applied moment is given by

$$\mu(\tau) = \bar{\mu}\cos(\Omega\tau), \tag{26}$$

where $\bar{\mu}$ is the non-dimensional magnitude of the applied moment and Ω is the non-dimensional frequency of the applied moment. To start, the constants in the system are set as follows: $L_c = 0.6$, $L_p = 0.4$, $M_a = 0.5$, $\gamma = 0.1$, $\gamma_a = 25$, $K_a = 12.5$, $K_i = 3$, $K_p = 10$. Eqs. (23)–(25) are integrated numerically using the Dormand-Prince method, which is a type of the Runge-Kutta ODE solver [24]. A tolerance of 10^{-7} was used when evaluating the Dormand-Prince method. This method is a standard method used to evaluate non-stiff equations with medium accuracy.

Since the reference forced pendulum is a two-state non-autonomous system, the system will exhibit either periodic motion or chaotic motion depending on the values of the parameters, see [25]. The hybrid forced pendulum is a five-state non-autonomous system and will also exhibit either periodic or chaotic motion. If the motion is periodic, the period of the steady-state motion will be an integer multiple of the forcing period, nT, where $n = 1, 2, 3\ldots$ and $T = \frac{2\pi}{\Omega}$; if $n > 1$, this corresponds to an excited subharmonic of period nT (see [26]). In order to determine the character of the motion of the systems, it is useful to employ the use of Lyapunov exponents; see [27]. If the largest Lyapunov exponent is positive, then the system will exhibit chaotic motion. If the largest Lyapunov exponent is 0, then the system will experience periodic motion; see [28]. Also, as long as the sum of all of the Lyapunov exponents is negative, then we know that the system is stable in the sense of Lyapunov. The Lyapunov exponents are found using the QR method for small continuous nonlinear systems as outlined by [29] and the FORTRAN code provided by [30] – LESNLS – was modified to calculate the Lyapunov exponents for our systems. For a thorough discussion on the utility and implementation of the LESNLS code, please see Dieci et al. [29].

To begin, let us examine how the magnitude of the applied moment determines the behavior of the responses of both the reference and hybrid systems for a fixed frequency of the applied moment. We will set $\Omega = 1$ for multiple values of $\bar{\mu}$. From this, we will be able to determine when the systems are either periodic or chaotic. Fig. 6 shows the largest Lyapunov exponent for the reference and hybrid systems as a function of the forcing magnitude. From Fig. 6 we can see that, for the most part, the reference and hybrid systems exhibit the same type of behavior. However, there are a few instances when one system is periodic and the other is chaotic. This indicates that there are three separate cases that one needs to consider when performing an error analysis of a nonlinear hybrid simulation system: both responses are periodic, both responses are chaotic, and one response is periodic while the other is chaotic.

4.1. Periodic reference and hybrid systems

First we will analyze the case when both the reference and hybrid systems are periodic. For this case, we attempt to utilize L^2 error to gauge how well the hybrid system is matching the reference system in the same manner as [16]. The L^2 error is given by

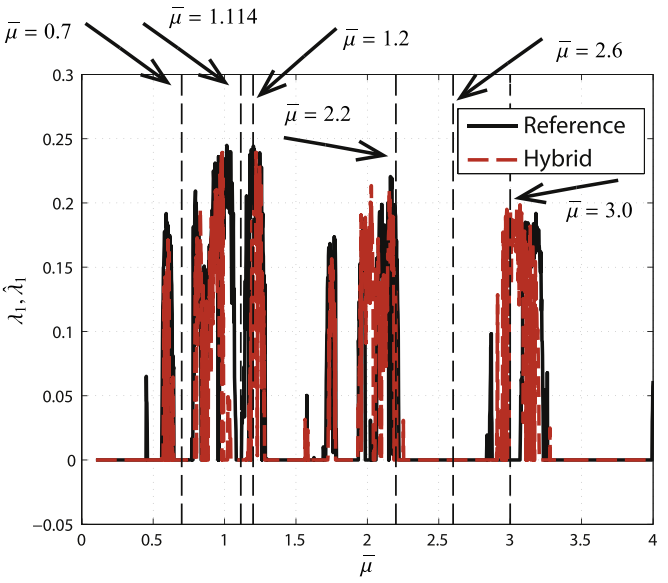

Fig. 6. The Lyapunov exponents for the reference, λ_1, and hybrid systems, $\hat{\lambda}_1$, when $\Omega = 1$.

$$E_2(\tau) = \frac{\sqrt{\int_0^\tau L_c\left((\theta-\theta_c)^2 + \left(\frac{d\theta}{d\tau} - \frac{d\theta_c}{d\tau}\right)^2\right) + L_p\left((\theta-\theta_p)^2 + \left(\frac{d\theta}{d\tau} - \frac{d\theta_p}{d\tau}\right)^2\right)}}{\sqrt{\int_0^\tau \theta^2 + \left(\frac{d\theta}{d\tau}\right)^2}}. \tag{27}$$

Note that the L^2 error used for the analysis is normalized with respect to the reference system. Also note that the difference in angles is always taken to be the smallest angular distance between 0 and 2π. We calculate the L^2 error at three different values of $\bar{\mu}$: $\bar{\mu} = 0.7,\ 1.114,\ 2.6$. A careful examination of Fig. 6 shows that all three of these values will produce periodic motion in both systems. The L^2 error time series for these three values of $\bar{\mu}$ are shown in Fig. 7. This figure shows that when the transients are still present, small τ, the error varies rapidly. However, as τ increases, the error approaches a steady state value. This makes sense because both systems are approaching a periodic solution, thus the difference between the two solutions should be approximately constant. However, as can be seen in Fig. 7, for $\bar{\mu} = 1.114$, the L^2 error approaches a value near 1.3, or 130%. This indicates that the hybrid system is not tracking the reference system at all. Upon further study we find that the reference system is traveling in a clockwise direction, while the hybrid system is traveling in a counter-clockwise direction. Thus, the hybrid system is matching the response of the reference system, just in the opposite direction. This is the

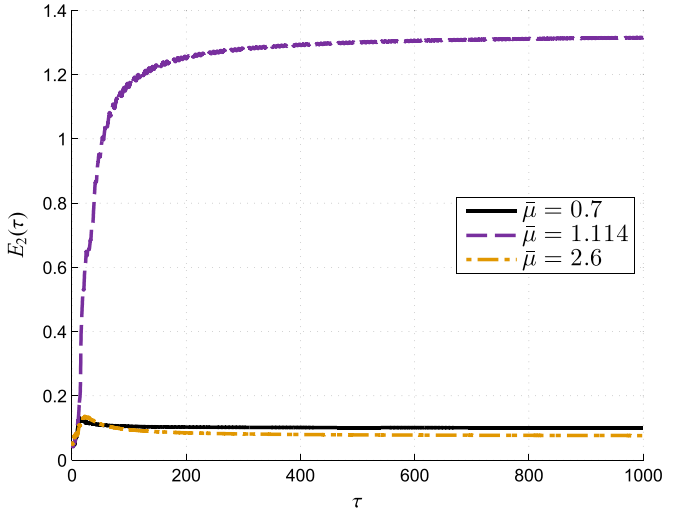

Fig. 7. The L^2 error for $\Omega = 1$ for three values of $\bar{\mu}$ with only periodic responses.

Please cite this article as: P.L. Drazin, & S. Govindjee, Hybrid simulation theory for a classical nonlinear dynamical system, *Journal of Sound and Vibration* (2016), http://dx.doi.org/10.1016/j.jsv.2016.12.034

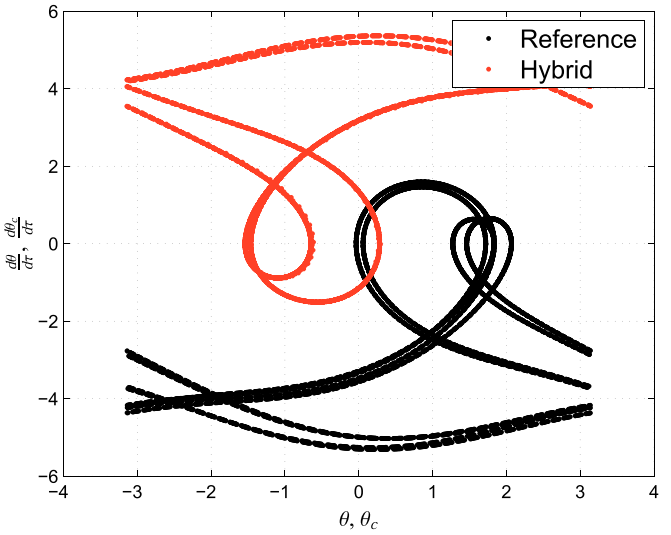

Fig. 8. The state space trajectories for the reference and hybrid systems with $\bar{\mu} = 1.114$.

cause of the large L^2 error. In order to more fully study the dynamical response, we can look at the state space of the two systems, which is shown Fig. 8. Note, only θ_c and $\frac{d\theta_c}{d\tau}$ are plotted for clarity in the figures (see Appendix A for similar plots for θ_p and $\frac{d\theta_p}{d\tau}$). From this figure, we can see that the state space trajectories are similar in shape, but vary by a rotation in state space. Thus, as long as the exact trajectory is not required, the hybrid response can be useful in understanding the dynamics of the reference system. Note that Fig. 8 also clearly shows that subharmonics are being excited in this case.

4.2. Chaotic reference and hybrid systems

Next we will analyze the case when both systems are chaotic. For the chaotic systems, the L^2 error is no longer a good metric for determining the error in the system. Instead, we will need to compare multiple aspects of the dynamics to fully understand the relationship between the reference and hybrid systems. First, we compare the systems visually before comparing them with error metrics. The time series, specifically, the angular velocity time series, is used to make a visual comparison of the reference and hybrid systems. We then compare the Poincaré Sections of the reference and hybrid systems. Note, for the plotting the Poincaré Sections, the time series was calculated out to $\tau = 10000$, and with $\Omega = 1$, this gives just under 1600 points per Poincaré Section. This allows us to compare the nature of the response on a more fundamental level. Two values of $\bar{\mu}$ are chosen for the chaotic case: $\bar{\mu} = 1.2,\ 2.2$. Again, Fig. 6 shows that these values will produce chaotic responses in both systems.

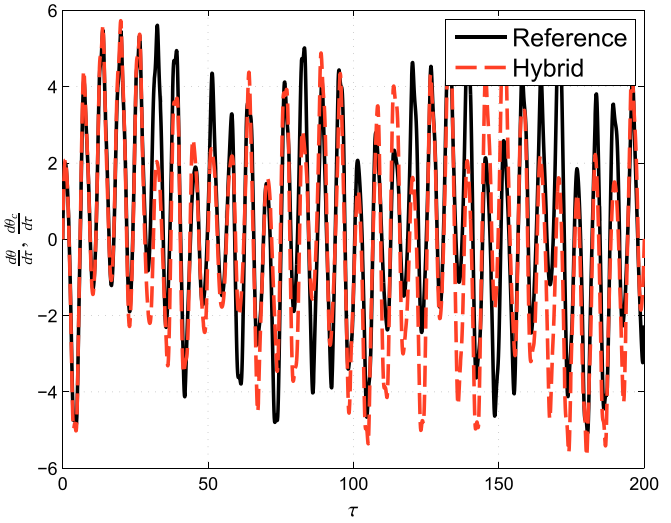

Fig. 9. The angular velocity time series of the reference and hybrid systems for $\bar{\mu} = 1.2$.

Please cite this article as: P.L. Drazin, & S. Govindjee, Hybrid simulation theory for a classical nonlinear dynamical system, *Journal of Sound and Vibration* (2016), http://dx.doi.org/10.1016/j.jsv.2016.12.034

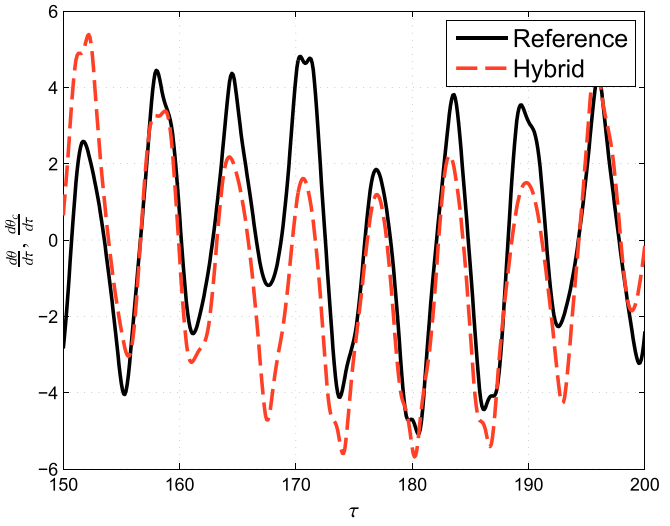

Fig. 10. A zoomed in plot of the angular velocity time series of the reference and hybrid systems for $\bar{\mu} = 1.2$.

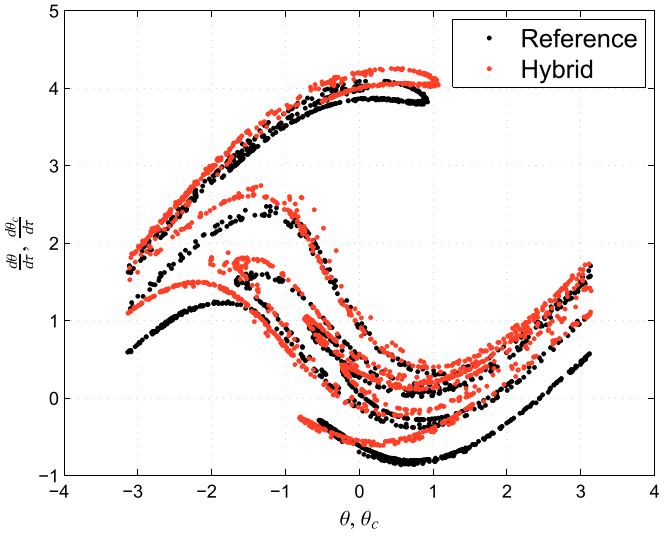

Fig. 11. The Poincaré Sections of the reference and hybrid systems for $\bar{\mu} = 1.2$.

Figs. 9 and 10 show the times series (of the angular velocities) for the systems with $\bar{\mu} = 1.2$ (see Appendix A for $\frac{d\theta_p}{d\tau}$ plots). It is clear that the two systems do not track each other very well. However, looking at Fig. 11, which shows the Poincaré Sections for both the reference and hybrid systems with $\bar{\mu} = 1.2$, we can easily see the similarity between the two Poincaré Sections. This indicates that even when both systems are chaotic, the fundamental nature of the responses are nearly identical.

Next, we look at the case when $\bar{\mu} = 2.2$. The angular velocity time series are shown in Figs. 12 and 13, which show that the time series of the reference and hybrid systems match each other fairly well. However, the corresponding Poincaré Sections, shown in Fig. 14, show very little correlation. Similar conclusions can be drawn from θ_p and $\frac{d\theta_p}{d\tau}$ as shown in Appendix A. So, even though the time series match well, their Poincaré Sections do not. This confirms the need to examine multiple aspects of the dynamics.

4.2.1. *Chaos error metrics*

Besides the above described visual error analysis, we compute three different error metrics used to give a numerical value to the error between two chaotic systems. First, we will compare Lyapunov exponents of the two systems. This allows us to directly compare the level of chaos in each system, as the Lyapunov exponent defines how quickly trajectories will diverge from each other due to small variations in the trajectories; see [31]. The second value we will compare is the Lyapunov dimension, d_L, which defines the *dimension* of the strange attractor and is calculated by

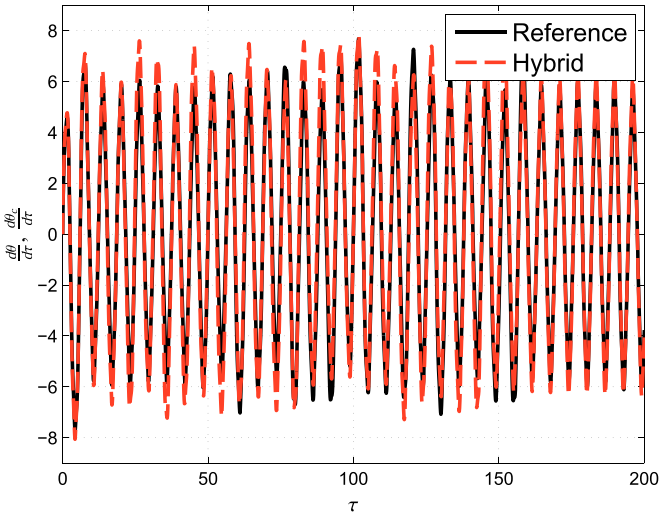

Fig. 12. The angular velocity time series of the reference and hybrid systems for $\bar{\mu} = 2.2$.

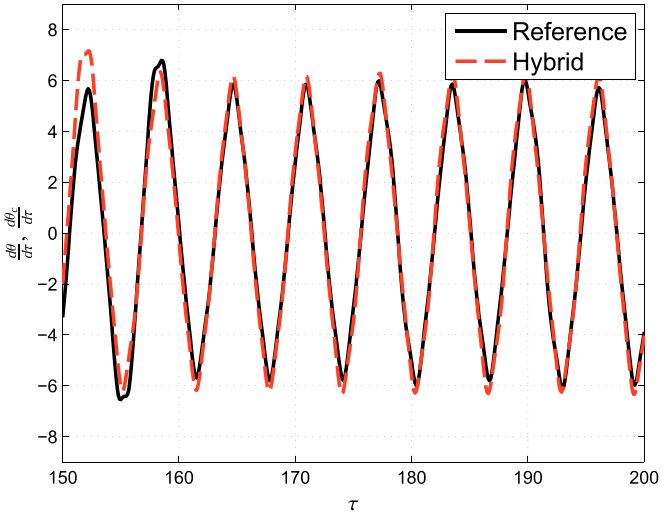

Fig. 13. A zoomed in plot of the angular velocity time series of the reference and hybrid systems for $\bar{\mu} = 2.2$.

$$d_L = j + \frac{\lambda_1 + \lambda_2 + \cdots + \lambda_j}{|\lambda_{j+1}|}, \tag{28}$$

where j is the largest integer for which $\lambda_1 + \lambda_2 + \cdots + \lambda_j \geq 0$, see [32]. The Lyapunov dimension can be used to classify the complexity of a strange attractor, since a strange attractor will have a fractional dimension, whereas a non-strange attractor will have an integer dimension. For our systems $j=2$. Thirdly, we will employ the correlation exponent, ν. The correlation exponent is used to measure the local structure of a strange attractor or Poincaré Section; see [33,34]. The correlation exponent is based on how close the points on a strange attractor or Poincaré section are to one another, which is another measure for the complexity of a strange attractor or Poincaré Section. In order to compute the correlation exponent, we first calculate the correlation integral,

$$C(r) = \frac{1}{N^2} \sum_{i,j=1, i\neq j}^{N} H(r - |\mathbf{X}_i - \mathbf{X}_j|), \tag{29}$$

where $H(x)$ is the Heaviside function, r is the correlation radius, and $\mathbf{X}_i$ are the states of the system at the i-th time step. Then using the relation

$$C(r) \propto r^{\nu}, \tag{30}$$

Please cite this article as: P.L. Drazin, & S. Govindjee, Hybrid simulation theory for a classical nonlinear dynamical system, *Journal of Sound and Vibration* (2016), http://dx.doi.org/10.1016/j.jsv.2016.12.034

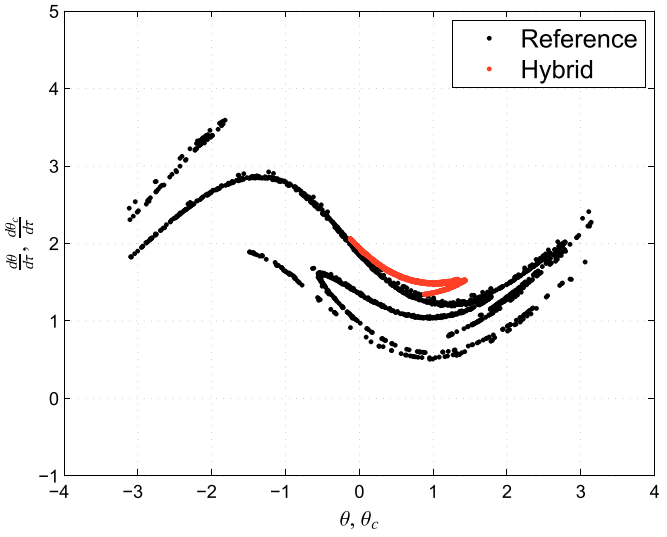

Fig. 14. The Poincaré Sections of the reference and hybrid systems for $\bar{\mu} = 2.2$.

we can solve for the correlation exponent, ν. In this paper, the correlation exponent was calculated using the points in the Poincaré Section. The errors with respect to these three metrics are calculated as follows:

$$err_{\lambda} = \frac{|\lambda_1 - \hat{\lambda}_1|}{\lambda_1}, \tag{31}$$

$$err_{d_L} = \frac{|d_L - \hat{d}_L|}{d_L}, \tag{32}$$

and

$$err_{\nu} = \frac{|\nu - \hat{\nu}|}{\nu}. \tag{33}$$

where the hat, $\hat{\bullet}$, again, represents quantities for the hybrid system. Figs. 15–17 show these error measures versus applied moment magnitude. Note, points are only calculated for values of $\bar{\mu}$ for which both the reference and hybrid system are chaotic.

Examining Fig. 15, we can see a wide variety of errors in the largest Lyapunov exponents, however, about half of all errors are less than 0.2, or less than 20 %. This shows that about half the time the levels of chaos in both systems are equivalent, yet

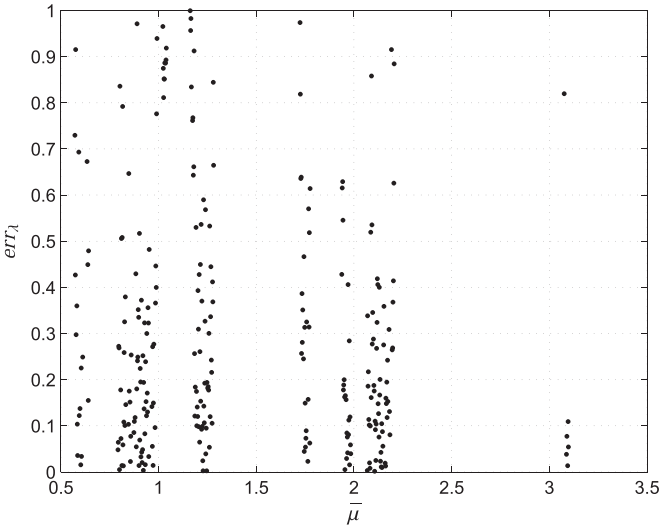

Fig. 15. The error between λ_1 and $\hat{\lambda}_1$ as a function of $\bar{\mu}$.

Please cite this article as: P.L. Drazin, & S. Govindjee, Hybrid simulation theory for a classical nonlinear dynamical system, *Journal of Sound and Vibration* (2016), http://dx.doi.org/10.1016/j.jsv.2016.12.034

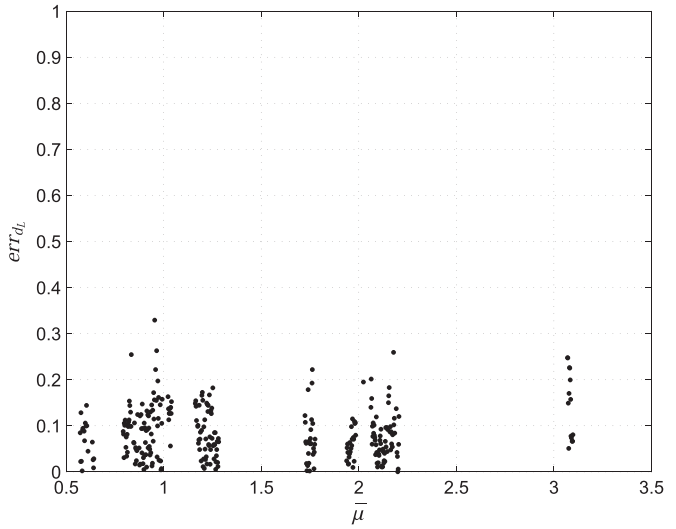

Fig. 16. The error in the Lyapunov dimension as a function of $\bar{\mu}$.

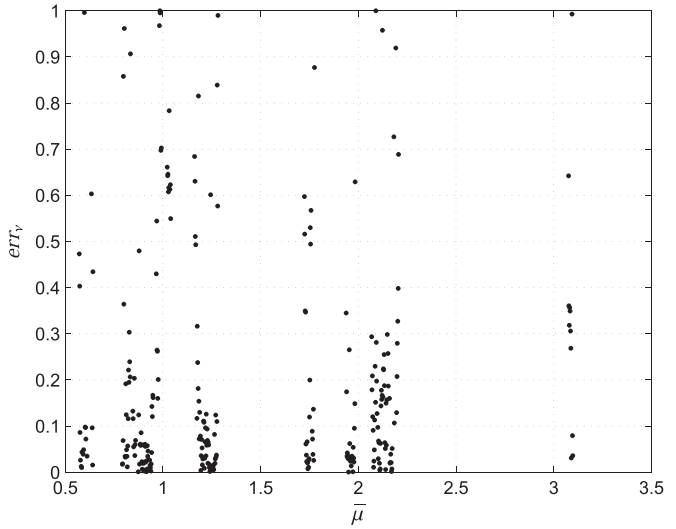

Fig. 17. The error in the correlation exponent of the Poincaré Sections as a function of $\bar{\mu}$.

there are times when the two systems vary greatly. Looking at Fig. 16, we see that all of the errors are below 0.4, and a significant portion, more than nine-tenths, are less than 0.2. This shows that there is much less deviation between the Lyapunov dimension of the reference and hybrid systems, indicating that the dimension of their strange attractors stay near one another. From examining Fig. 17, we can see that there is a high density of points below 0.2, about two-thirds of all points are below 0.2. This shows that most of the time the Poincaré Sections of the two systems match fairly well, however, there are still instances in which the two systems do not match well. For the cases which we visually examined above, $err_{\lambda_1} = 0.1203$, $err_{d_L} = 0.1552$, and $err_\nu = 0.0526$ when $\bar{\mu} = 1.2$, and $err_{\lambda_1} = 0.3680$, $err_{d_L} = 2.810 \times 10^{-4}$, and $err_\nu = 0.2792$ for $\bar{\mu} = 2.2$. These values again fit with our determination that multiple quantities are needed to properly assess the error between two chaotic responses.

4.3. One system periodic and the other chaotic

The third case is when one system has a chaotic response and the other system has a periodic response. In this situation it is not possible to compare the two systems as the L^2 error breaks down for chaotic systems, and the Poincaré Section for a periodic system will be a single point, whereas the Poincaré Section for a chaotic system will be Cantor-like, see e.g. [35] or [25]. For these reasons, it is clear the correlation between the two responses will be nonexistent.

Please cite this article as: P.L. Drazin, & S. Govindjee, Hybrid simulation theory for a classical nonlinear dynamical system, *Journal of Sound and Vibration* (2016), http://dx.doi.org/10.1016/j.jsv.2016.12.034

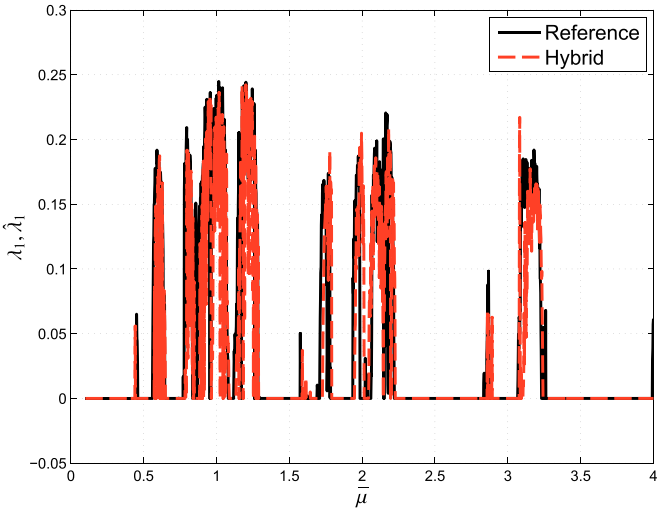

Fig. 18. The Lyapunov exponents for the reference and hybrid systems when $K_i=10$.

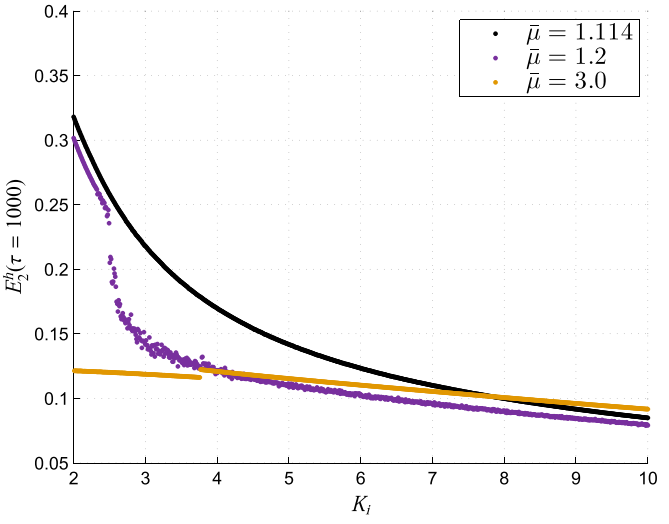

Fig. 19. The E_2^h error as a function of K_i for multiple values of $\bar{\mu}$.

4.4. Study of K_i

All of the above analysis was done with specific values of the control parameters. If we instead use $K_i=10$, which was arbitrarily chosen, we can see how the Lyapunov exponents of the hybrid system match those of the reference system much better, as seen by comparing Figs. 6 and 18. This potentially indicates that if we increase the integral gain, K_i, we get better matching between the reference and hybrid systems. To investigate this further, we now look at the effects of changing the integral gain, K_i. In the context of this paper, holding K_p constant and increasing K_i means the response of the controlled system is quicker, but it becomes more oscillatory and less stable [22]. Thus, as K_i increases, the magnitude error at the hybrid interface increases while the phase error decreases. However, it is noted that this only applies for the simple PI controller used in this paper. We will look at three specific values of $\bar{\mu}$:$\bar{\mu}$ = 1.114, 1.2, 3.0. The first value was chosen because both the hybrid and reference systems were periodic at $K_i=3$, but the hybrid system is going the opposite direction of the reference system. The second value was chosen because the response is chaotic for both systems at $K_i=3$. And the third value was chosen because the reference response is periodic, while the hybrid response is chaotic at $K_i=3$. For analyzing the effect of changing K_i, we look at the hybrid L^2 error once the transients have died out and the error has reached steady state:

Please cite this article as: P.L. Drazin, & S. Govindjee, Hybrid simulation theory for a classical nonlinear dynamical system, *Journal of Sound and Vibration* (2016), http://dx.doi.org/10.1016/j.jsv.2016.12.034

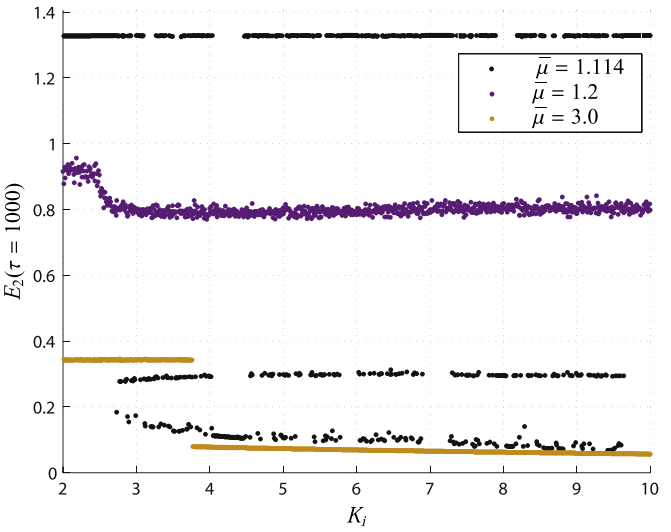

Fig. 20. The E_2 error as a function of K_i for multiple values of $\bar{\mu}$.

$$E_2^h(\tau = 1000) = \frac{\sqrt{\int_0^\tau \left(\theta_c - \theta_p\right)^2 + \left(\frac{d\theta_c}{d\tau} - \frac{d\theta_p}{d\tau}\right)^2}}{\sqrt{\int_0^\tau \theta_c^2 + \left(\frac{d\theta_c}{d\tau}\right)^2}}. \tag{34}$$

Note that E_2^h is normalized to the top piece of the hybrid pendulum. The hybrid L^2 error determines how well the two pieces of the hybrid pendulum are matching each other and is an error measure we can apply independent of the chaotic or periodic nature of either system. As we can see from Fig. 19, as K_i is increased, the hybrid L^2 error decreases for all three values of $\bar{\mu}$, which makes sense because K_i affects the the steady state response, thus the two pieces should match better for larger values of K_i, see [22]. However, if we look at the steady state L^2 error in Fig. 20, we see that the L^2 error does not decrease as K_i is increased, in fact, all three values of $\bar{\mu}$ have different responses to increasing K_i.

For $\bar{\mu} = 1.114$ we see that the error approximately goes between three values as K_i increases. This indicates that even though the hybrid pieces are matching each other better, the hybrid pendulum is not always matching the reference pendulum better. In fact, the highest value represents the hybrid pendulum spinning in the opposite direction of the reference pendulum, the middle value represents the hybrid pendulum spinning in the same direction as the reference pendulum, but taking a long time to reach the steady-state solution, and the low value represents the hybrid pendulum spinning in the same direction as the reference pendulum and reaching the steady-state solution more quickly.

For $\bar{\mu} = 1.2$, the L^2 error is not a good metric for analyzing the error. Instead, we again look at the Poincaré Sections, as shown in Fig. 21 (see Appendix A for θ_p and $\frac{d\theta_p}{d\tau}$ plots). From a close comparison of Figs. 11 and 21, we can see that with $K_i = 10$, the Poincaré Sections match better than when $K_i = 3$. This indicates that the hybrid response is better for larger values of K_i. Evaluating the error metrics from before, we find that $err_{\lambda_1} = 0.5722$, $err_{d_L} = 0.0919$, and $err_\nu = 0.0332$. Comparing these values to those found before, we find that the Lyapunov dimension error and correlation exponent error have decreased, while the Lyapunov exponent error has increased. This again indicates the need for multiple metrics to gauge the chaotic response because even though it appears that increasing K_i made the hybrid response better, there is actually a metric in which it became worse.

Finally, for $\bar{\mu} = 3.0$, the L^2 error sharply drops around $K_i = 4$. This occurs because the hybrid system changes from chaotic to periodic, while the reference system is periodic throughout. After the transition, the hybrid system has the same response type as the reference system. The L^2 error stays low because the hybrid system is traveling in the same direction as the reference system, and does not change direction, unlike the case of $\bar{\mu} = 1.114$. This confirms, for the most part, the conclusion about the usage of K_i reached from Fig. 18.

5. Discussion

From analyzing the reference and hybrid systems, we see that there are there are three unique cases that can arise when considering the responses of the reference and hybrid systems: (1) both responses are periodic, (2) both responses are

Please cite this article as: P.L. Drazin, & S. Govindjee, Hybrid simulation theory for a classical nonlinear dynamical system, *Journal of Sound and Vibration* (2016), http://dx.doi.org/10.1016/j.jsv.2016.12.034

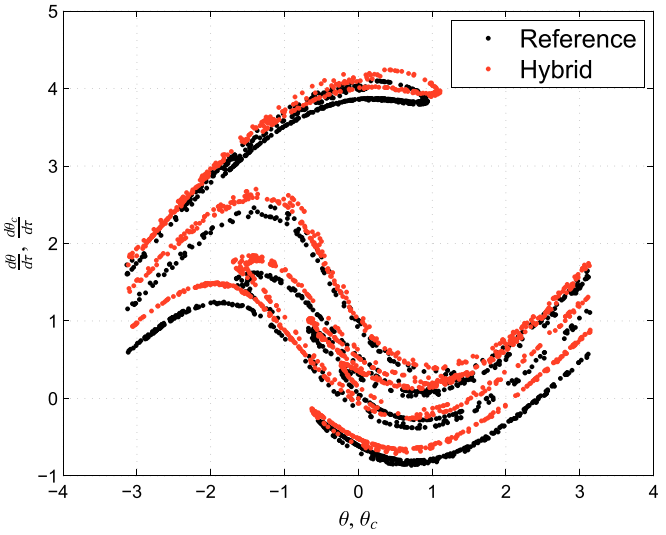

Fig. 21. The Poincaré Sections of the reference and hybrid systems for $\bar{\mu} = 1.2$ and $K_i = 10$.

chaotic, and (3) one response is periodic while the other is chaotic.

1. For the periodic-periodic case, we see that sometimes the hybrid system tracks the reference system well, low L^2 error, and other times it does not track the reference system well, high L^2 error. However, in the case of high L^2 error, we note that the two systems experience similar motions, despite not tracking well, which is shown in Fig. 8. This leads to a fundamental question of hybrid simulation: what does one expect to get from hybrid simulation? If one hopes to get perfect tracking with hybrid simulation, while it is possible via adjustment of the control parameters, it is not to be expected or assumed with a *nonlinear* system, and thus hybrid simulation loses its utility if perfect tracking is the goal. If one wishes to understand the general response of the dynamical system in that the same parts of the phase space are traversed and at the same frequency, then hybrid simulation can still be useful, and the hybrid system can provide a good representation of the reference system response. Put another way, if one is content that the hybrid system experiences the same states as the true system, independent of temporal ordering, then hybrid simulation retains its utility in the nonlinear setting.
2. This trend carries into the second case, where both systems are chaotic. In the first example – $\bar{\mu} = 1.2$ – we observe poor time series matching but a good matching of Poincaré Sections, indicating a clear correlation in the dynamics of the two systems. And in the second example – $\bar{\mu} = 2.2$ – we find good time series matching, but little correlation between the two Poincaré sections. Thus, we note a need to compare more than one aspect of the dynamics, for example the largest Lyapunov exponents, the Lyapunov dimension, and the correlation exponent can be used to analyze the correspondence between the responses. Using Fig. 11, it is clear that responses are similar. Even though the time series of the reference and hybrid systems do not follow each other closely, the allowable motions for each system are closely related. Using Figs. 12 and 13, it is clear that the time series match well even though the Poincaré Sections are not similar, which still indicates that responses of the reference and hybrid systems are correlated in the example. Thus, knowing the response of the hybrid system does give an approximation of how the reference system will respond. Again, as long as the exact trajectory is not needed, i.e. one is satisfied that the system moves through the correct states at the correct sampling frequency, then hybrid simulation is still useful for understanding the response of the reference system. This information linked with the numerical error metrics agrees with the conclusion made in the first case, in that one needs to be fully aware of what one wants from hybrid simulation; exact matching may not be possible, however, it is possible for hybrid simulation to properly reproduce certain dynamical quantities, which can be just as useful.
3. Finally, for the third case – one system is periodic and the other is chaotic – it is not useful to try and compare the two responses. For the periodic system, the response will approach a periodic steady-state, whereas in the chaotic system, the response will be an aperiodic solution. Thus all of the errors discussed in this paper will indicate large differences in the behavior of the response.

The three cases discussed were all examined within the context with a single value of the integral gain, K_i, specifically $K_i = 3$. However, upon changing K_i we are able to understand more about the nature of the hybrid response. In all cases, the error internal to the hybrid system, $E_2^h(\tau = 1000)$, decreases as K_i is increased. Unfortunately, this does not directly translate to better

Please cite this article as: P.L. Drazin, & S. Govindjee, Hybrid simulation theory for a classical nonlinear dynamical system, *Journal of Sound and Vibration* (2016), http://dx.doi.org/10.1016/j.jsv.2016.12.034

tracking between the hybrid and reference systems as seen, for example, by comparing Figs. 19 and 20. In the case when both systems are periodic, it is possible, as K_i increases, for the hybrid system to change from a counter-clockwise rotation to a clockwise rotation and back. Notwithstanding, in almost all other instances, increasing K_i produces a better hybrid result. However, one can not simply increase the value of K_i to whatever one wishes, there are stability and physical constraints that determine the feasible range of K_i, thus understanding how to effectively use the control parameters is of great importance and here we have only examined one very simple control system since the underlying set of outcomes is independent of this choice and better controllers will not obviate the need to understand chaotic trajectories in the nonlinear case.

6. Conclusions

This paper focused on the fundamental interface mismatch error that occurs during *nonlinear* hybrid simulation. To study this intrinsic error we examined the behavior of a kinematically nonlinear hybrid system with a spring-mass-damper actuator system, controlled by a PI controller. This is a relatively simple model, but it gave us a lot of control over the study of our system. Most importantly, the setup was entirely theoretical and provided a true reference against which we could compare hybrid results. In particular we have found that:

1. In the nonlinear setting, hybrid simulation must account for three separate cases where the hybrid system and true system can separately take on either periodic or chaotic behavior.
2. The minimization of internal (interface) error does not necessarily mean that a hybrid system will faithfully track the true system response.
3. When good tracking does not occur, we find that hybrid simulation can still be useful if one modifies one's objective to the notion that the hybrid system should move through the same parts of the system's state space at the same relative frequency.
4. In the case of chaotic system response, one needs to employ multiple metrics to ensure adequate accuracy.

Overall, we conclude that the application of hybrid simulation to nonlinear systems is a delicate matter requiring an understanding of what one wishes to achieve, a knowledge of the three possible outcomes, and the application of multiple metrics to ensure fidelity.

Appendix A. θ_p and $\frac{d\theta_p}{d\tau}$ Plots

In the main body of the text we consistently compare the dynamical response of the $\mathcal{C}$ part of the hybrid system to the reference system. In this appendix we provide comparison plots using the dynamical response of the $\mathcal{P}$ part. This is provided for completeness. All conclusions made from the plots in the main body of the text remain true (Figs. A.22–A.29).

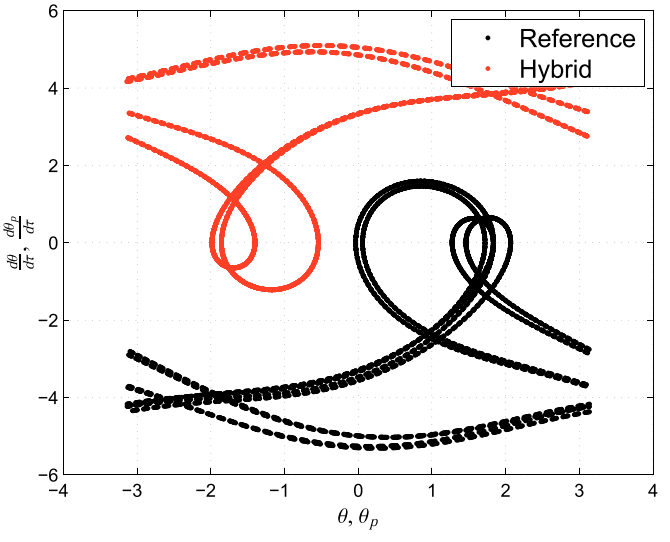

Fig. A.22. The state space trajectories for the reference and hybrid systems with $\bar{\mu} = 1.114$. Compare to Fig. 8.

Please cite this article as: P.L. Drazin, & S. Govindjee, Hybrid simulation theory for a classical nonlinear dynamical system, *Journal of Sound and Vibration* (2016), http://dx.doi.org/10.1016/j.jsv.2016.12.034

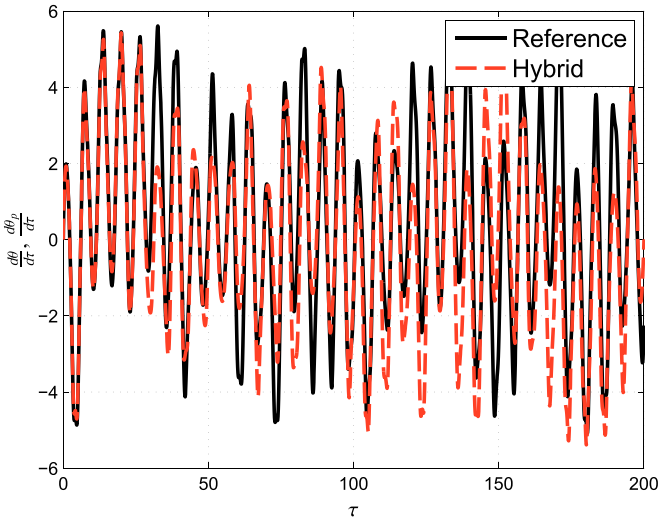

Fig. A.23. The angular velocity time series of the reference and hybrid systems for $\bar{\mu} = 1.2$. Compare to Fig. 9.

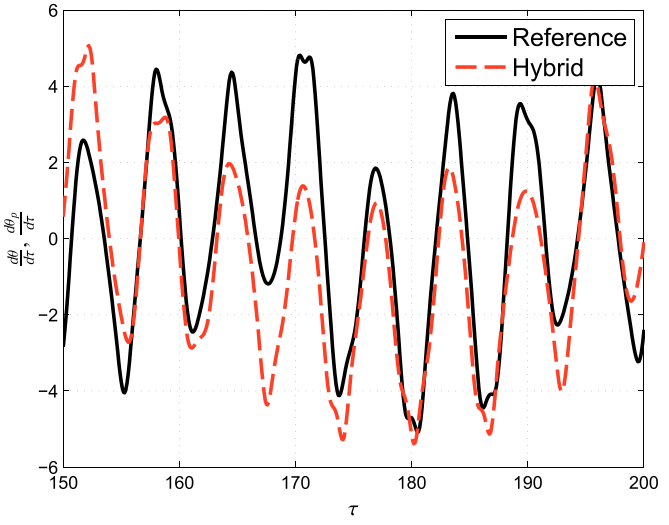

Fig. A.24. A zoomed in plot of the angular velocity time series of the reference and hybrid systems for $\bar{\mu} = 1.2$. Compare to Fig. 10.

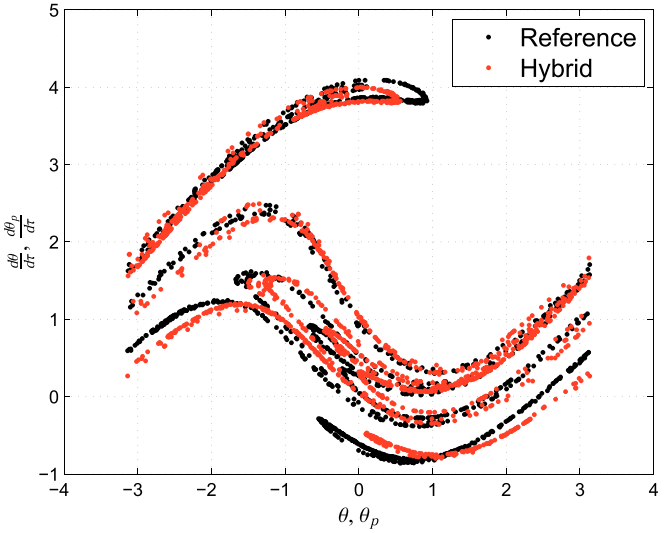

Fig. A.25. The Poincaré Sections of the reference and hybrid systems for $\bar{\mu} = 1.2$. Compare to Fig. 11.

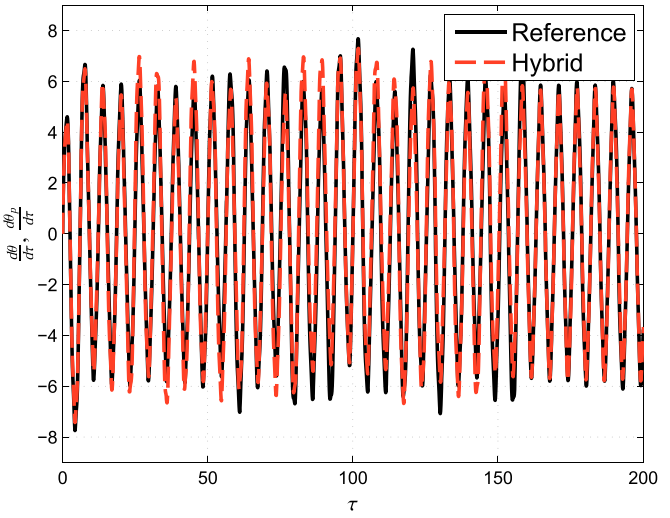

Fig. A.26. The angular velocity time series of the reference and hybrid systems for $\bar{\mu} = 2.2$. Compare to Fig. 12.

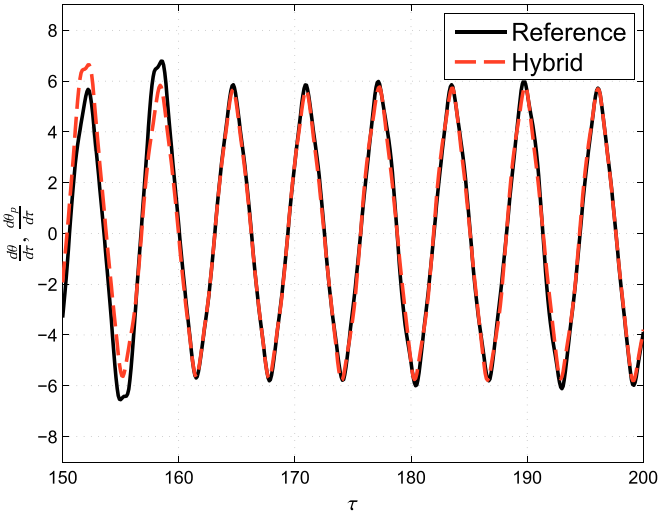

Fig. A.27. A zoomed in plot of the angular velocity time series of the reference and hybrid systems for $\bar{\mu} = 2.2$. Compare to Fig. 13.

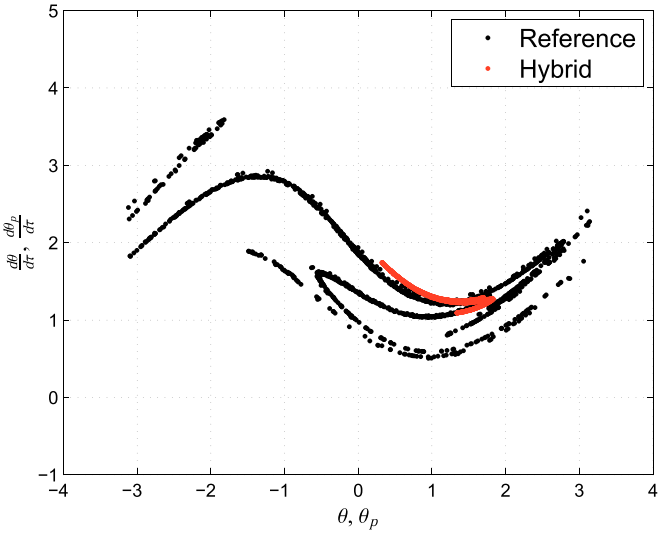

Fig. A.28. The Poincaré Sections of the reference and hybrid systems for $\bar{\mu} = 2.2$. Compare to Fig. 14.

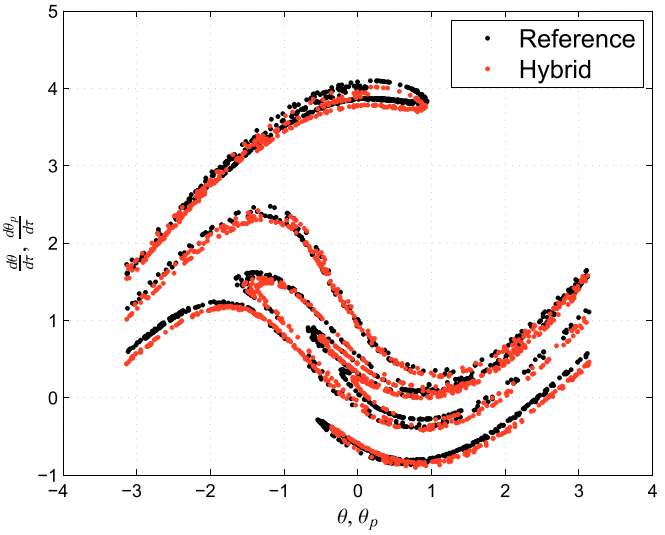

Fig. A.29. The Poincaré Sections of the reference and hybrid systems for $\bar{\mu} = 1.2$ and $K_i = 10$. Compare to Fig. 21.

References

[1] P.S.B. Shing, S.A. Mahin, Pseudodynamic test method for seismic performance evaluation: theory and implementation., Tech. Rep. UCB-EERC-84-01, Earthquake Engineering Research Center, Berkeley, CA, 1984.
[2] P.S.B. Shing, S.A. Mahin, Elimination of spurious higher-mode response in pseudodynamic tests, *Earthq. Eng. Struct. Dyn.* 15 (4) (1987) 409–424.
[3] K. Takanashi, M. Nakashima, Japanese activities on on-line testing, *J. Eng. Mech.* 113 (7) (1987) 1014–1032.
[4] O.S. Bursi, C. Jia, L. Vulcan, S.A. Neild, D.J. Wagg, Rosenbrock-based algorithms and subcycling strategies for real-time nonlinear substructure testing, *Earthq. Eng. Struct. Dyn.* 40 (1) (2011) 1–19.
[5] M. Verma, J. Rajasankar, Improved model for real-time substructuring testing system, *Eng. Struct.* 41 (2012) 258–269.
[6] M. Zapateiro, H.R. Karimi, N. Luo, B.F. Spencer, Real-time hybrid testing of semiactive control strategies for vibration reduction in a structure with MR damper, *Struct. Control Health Monit.* 17 (4) (2010) 427–451.
[7] E-defense, ⟨http://www.bosai.go.jp/hyogo/ehyogo/profile/introduction/Introduction.html⟩, (Online accessed 08.06.16).
[8] A.H. Schellenberg, Advanced Implementation of Hybrid Simulation (Ph.D. thesis), University of California, Berkeley, CA, 2008.
[9] D. McCrum, M. Williams, An overview of seismic hybrid testing of engineering structures, *Eng. Struct.* 118 (2016) 240–261.
[10] M.S. Williams, A. Blakeborough, Laboratory testing of structures under dynamic loads: an introductory review, *Philos. Trans. R. Soc. Lond. A: Math. Phys. Eng. Sci.* 359 (1786) (2001) 1651–1669.
[11] K.M. Mosalam, S. Günay, Seismic performance evaluation of high voltage disconnect switches using real-time hybrid simulation: I. System development and validation, *Earthq. Eng. Struct. Dyn.* 43 (8) (2014) 1205–1222.
[12] A.P. Darby, A. Blakeborough, M.S. Williams, Improved control algorithm for real-time substructure testing, *Earthq. Eng. Struct. Dyn.* 30 (3) (2001) 431–448.
[13] D. Wagg, S. Neild, P. Gawthrop, Real-time testing with dynamic substructuring, in: O.S. Bursi, D. Wagg (Eds.), Modern Testing Techniques for Structural Systems: Dynamics and Control, Springer Vienna, Vienna, 2008, pp. 293–342.
[14] C. Chen, J.M. Ricles, Tracking error-based servohydraulic actuator adaptive compensation for real-time hybrid simulation, *J. Struct. Eng.* 136 (4) (2010) 432–440.
[15] N. Terkovics, S.A. Neild, M. Lowenberg, R. Szalai, B. Krauskopf, Substructurability: the effect of interface location on a real-time dynamic substructuring test, Proc. R. Soc. Lond. A: Math. Phys. Eng. Sci., 472, 2192.
[16] P.L. Drazin, S. Govindjee, K.M. Mosalam, Hybrid simulation theory for continuous beams, *ASCE J. Eng. Mech.* 141 (7) (2015) 04015005.
[17] A.A. Bakhaty, S. Govindjee, K.M. Mosalam, Theoretical development of hybrid simulation applied to plate structures, Tech. Rep. UCB-PEER-2014-02, Pacific Earthquake Engineering Research Center, Berkeley, CA, 2014.
[18] S.N. Voormeeren, D. de Klerk, D.J. Rixen, Uncertainty quantification in experimental frequency based substructuring, *Mech. Syst. Signal Process.* 24 (1) (2010) 106–118.
[19] G.L. Baker, J.A. Blackburn, *The Pendulum: A Case Study in Physics*, Oxford University Press, New York, 2005.
[20] M. Ahmadizadeh, G. Mosqueda, A.M. Reinhorn, Compensation of actuator delay and dynamics for real time hybrid structural simulation, *Earthq. Eng. Struct. Dyn.* 37 (1) (2008) 21–42.
[21] O.M. O'Reilly, *Intermediate Dynamics for Engineers*, Cambridge University Press, New York, 2008.
[22] N.S. Nise, *Control Systems Engineering*, John Wiley & Sons, New York, 2008.
[23] T. Elkhoraibi, K.M. Mosalam, Towards error-free hybrid simulation using mixed variables, *Earthq. Eng. Struct. Dyn.* 36 (11) (2007) 1497–1522.
[24] J. Dormand, P. Prince, A family of embedded Runge-Kutta formulae, *J. Comput. Appl. Math.* 6 (1) (1980) 19–26.
[25] T.S. Parker, L.O. Chua, *Practical Numerical Algorithms for Chaotic Systems*, Springer-Verlag, New York, 1989.
[26] J. Guckenheimer, P. Holmes, *Nonlinear Oscillations, Dynamical Systems, and Bifurcations of Vector Fields*, Springer-Verlag, New York, 1983.
[27] A.H. Nayfeh, B. Balachandran, *Applied Nonlinear Dynamics*, John Wiley & Sons, New York, 1995.
[28] G.L. Baker, J.P. Gollub, *Chaotic Dynamics: An Introduction*, Cambridge University Press, New York, 1996.
[29] L. Dieci, M.S. Jolly, E.S. Van Vleck, Numerical techniques for approximating Lyapunov exponents and their implementation, *J. Comput. Nonlinear Dyn.* 6 (1) . 011003-011003-7.
[30] L. Dieci, E.S. Van Vleck, Software: LESLIS/LESLIL and LESNLS/LESNLL, ⟨http://www.math.gatech.edu/~dieci/software-les.html⟩, (Online accessed 03.02.15).
[31] R. Gilmore, M. Lefranc, *The Topology of Chaos*, Wiley-VCH, Weinheim, Germany, 2011.
[32] P. Frederickson, J.L. Kaplan, E.D. Yorke, J.A. Yorke, The Lyapunov dimension of strange attractors, *J. Differ. Equ.* 49 (2) (1983) 185–207.
[33] P. Grassberger, I. Procaccia, Characterization of strange attractors, *Phys. Rev. Lett.* 50 (5) (1983) 346–349.
[34] P. Grassberger, I. Procaccia, Measuring the strangeness of strange attractors, *Phys. D: Nonlinear Phenom.* 9 (1) (1983) 189–208.
[35] S.S. Rao, *Mechanical Vibrations*, Prentice Hall, Upper Saddle River, NJ, 2004.

Please cite this article as: P.L. Drazin, & S. Govindjee, Hybrid simulation theory for a classical nonlinear dynamical system, *Journal of Sound and Vibration* (2016), http://dx.doi.org/10.1016/j.jsv.2016.12.034